



**HAL**  
open science

## Coercivity enhancement in exchange biased CoO/Co<sub>3</sub>Pt bilayers

T Kosub, C Schubert, H Schletter, M Daniel, M Hietschold, V Neu, M Maret,  
D Makarov, M Albrecht

► **To cite this version:**

T Kosub, C Schubert, H Schletter, M Daniel, M Hietschold, et al.. Coercivity enhancement in exchange biased CoO/Co<sub>3</sub>Pt bilayers. *Journal of Physics D: Applied Physics*, 2011, 44 (1), pp.15002. 10.1088/0022-3727/44/1/015002 . hal-00585171

**HAL Id: hal-00585171**

**<https://hal.science/hal-00585171>**

Submitted on 12 Apr 2011

**HAL** is a multi-disciplinary open access archive for the deposit and dissemination of scientific research documents, whether they are published or not. The documents may come from teaching and research institutions in France or abroad, or from public or private research centers.

L'archive ouverte pluridisciplinaire **HAL**, est destinée au dépôt et à la diffusion de documents scientifiques de niveau recherche, publiés ou non, émanant des établissements d'enseignement et de recherche français ou étrangers, des laboratoires publics ou privés.

## Coercivity enhancement in exchange biased CoO/Co<sub>3</sub>Pt bilayers

T. Kosub<sup>1</sup>, C. Schubert<sup>1</sup>, H. Schletter<sup>1</sup>, M. Daniel<sup>1</sup>, M. Hietschold<sup>1</sup>, V. Neu<sup>2</sup>, M. Maret<sup>3</sup>, D. Makarov<sup>1a</sup>,  
and M. Albrecht<sup>1</sup>

<sup>1</sup> Institute of Physics, Chemnitz University of Technology, D-09107 Chemnitz, Germany

<sup>2</sup> Institute for Metallic Materials, IFW Dresden, D-01069 Dresden, Germany

<sup>3</sup> SIMAP, INP Grenoble-CNRS-UJF, BP75, F-38402 Saint Martin d'Hères, France

A study on the exchange bias effect in an hcp (0002)-textured Co<sub>3</sub>Pt alloy film biased by a thin CoO film is presented. The Co<sub>3</sub>Pt film reveals an out-of-plane easy axis of magnetization although it was grown on an amorphous silica substrate at room temperature. Similar exchange bias fields measured in in-plane and out-of-plane directions of the CoO/Co<sub>3</sub>Pt bilayer system were observed for maximum cooling field. Whereas a pronounced cooling field dependence of the exchange bias field is observed in-plane, it remains constant in out-of-plane direction. The temperature evolution of the coercivity and the shift of the hysteresis loop caused by the exchange bias effect are discussed in terms of thermal activation accounting for the temperature dependent competition between the interfacial exchange energy and the anisotropy energy of antiferromagnetic grains.

<sup>a</sup> Corresponding author: [denys.makarov@physik.tu-chemnitz.de](mailto:denys.makarov@physik.tu-chemnitz.de)

## Introduction

Discovered in 1956 as a unidirectional anisotropy [1], the exchange bias (EB) effect attracted much attention from a fundamental point of view and for applications in the field of sensorics. EB is a proximity effect appearing when a stack consisting of a ferromagnetic (F) and an antiferromagnetic (AF) layer is cooled through the Néel temperature of the AF layer in an applied magnetic field [2-4]. Usually EB is expressed in terms of the shift of the magnetic hysteresis loop and a modification of the coercive field of the F layer. The physical origin of EB is generally accepted to be the exchange coupling between the F and uncompensated AF spins at the F/AF interface. The microscopic way, in which this coupling translates into EB is more controversial and many models have been proposed [5-12].

So far most of the studies of the EB effect were focused on F films with in-plane (IP) easy axis of magnetization [4, 13, 14]. However, AF/F composites exhibiting an out-of-plane (OOP) exchange bias effect are rather attractive for applications in magnetic sensor devices operating in a current-perpendicular-to-plane geometry as they reveal superior signal-to-noise ratio compared to the current-in-plane sensors [15-19]. In this respect, only a few reports on OOP exchange bias systems are available [20-25]. Maat et al. [20] reported on the EB effect in Co/Pt multilayer stacks with strong perpendicular magnetic anisotropy (PMA) biased by a thin CoO AF layer. It was shown that CoO grown on (111)-textured [Co/Pt] multilayers results in an anisotropic exchange bias effect with substantially larger shift of the magnetic hysteresis loop in IP direction compared to the OOP one. In addition, the scaling dependence of the OOP exchange bias effect in nanostructures consisting of CoO or IrMn coupled to Co/Pd(Pt) deposited onto arrays of spherical nonmagnetic particles was recently investigated [21-23].

Here, we present a study of the exchange bias effect in a bilayer consisting of a 5-nm-thick Co<sub>3</sub>Pt alloy film with an out-of-plane easy axis of magnetization and a naturally oxidized 1-nm-thick Co layer. The cooling field dependence as well as the temperature dependence of the exchange bias field and the coercivity of the CoO/Co<sub>3</sub>Pt bilayer system will be discussed.

## Sample preparation and experimental techniques

5-nm-thick Co<sub>3</sub>Pt alloy films were prepared at room temperature on thermally oxidized Si(100) substrates with a 100-nm-thick amorphous SiO<sub>2</sub> layer. The deposition was carried out by dc-magnetron co-sputtering of Co and Pt in a high vacuum chamber with a base pressure of  $1 \times 10^{-6}$  mbar. Argon was used as a sputter gas at a pressure of  $3.5 \times 10^{-3}$  mbar. The composition of the alloy film was controlled by adjusting the deposition rates of Co (0.22 Å/s) and Pt (0.1 Å/s). A composition of Co<sub>x</sub>Pt<sub>100-x</sub> with  $x = (73 \pm 1)$  was

determined by Rutherford backscattering spectroscopy. These films serve as reference samples for further investigations. In addition, a series of CoO/Co<sub>3</sub>Pt film samples was prepared by introducing the initial film samples into the sputter chamber and depositing an additional 1-nm-thick Co layer followed by the oxidation of the Co layer at ambient conditions. Note that the Co<sub>3</sub>Pt samples were exposed to air before the Co layer deposition, which led to an oxidation of the top surface.

The structural characterization was carried out by x-ray diffraction (XRD) using Cu-K<sub>α</sub> radiation ( $\lambda = 1.5406 \text{ \AA}$ ), by atomic force microscopy (AFM), and by transmission electron microscopy (TEM) in both conventional and high resolution (HRTEM) modes employing a 200 kV Philips CM 20 FEG TEM.

Temperature dependent magnetic measurements were performed in IP and OOP geometry using a Quantum Design SQUID-VSM magnetometer. The measurement routine included a warming process to 320 K, which is above the Néel temperature,  $T_N = 290 \text{ K}$ , of bulk CoO. A maximum field of +70 kOe was applied to achieve complete saturation of the ferromagnetic Co<sub>3</sub>Pt layer. Then, the cooling field,  $H_{\text{cool}}$ , was set at 320 K. With the cooling field applied, the samples were cooled down to the desired measurement temperature,  $T_{\text{meas}}$ , at which the hysteresis loop was measured.  $T_{\text{meas}}$  and  $H_{\text{cool}}$  were varied over a wide range to investigate the dependence of coercivity,  $H_C$ , and exchange bias field,  $H_{\text{EB}}$ , on both parameters.

### Structural properties

The x-ray diffraction pattern of the Co<sub>3</sub>Pt film measured in  $\theta$ - $2\theta$  reflection geometry shows a single peak at  $\theta = 21.285^\circ$  (figure 1(a)). The position of the peak corresponds to an interplanar distance of  $2.122 \text{ \AA}$ , which is close to the value of the fcc (111) Co<sub>3</sub>Pt bulk alloy [26] and the one found in epitaxial hcp (0002) Co<sub>3</sub>Pt films [27-29]. The full width at half maximum of the peak leads to a perpendicular coherence length of 4.7 nm, which is slightly smaller than the nominal Co<sub>3</sub>Pt film thickness. The width of the corresponding rocking curve (RC) is equal to  $12^\circ$  (figure 1(a)). Such broadening of the rocking curve can be attributed to a small lateral size of the Co<sub>3</sub>Pt grains and/or high mosaicity. Neither reflections coming from oblique planes characteristic of the fcc or hcp stacking, nor a superstructure peak indicative of long-range chemical ordering as measured for epitaxial hcp Co<sub>3</sub>Pt films [27, 29] were observed.

The structural properties of the CoO/Co<sub>3</sub>Pt sample were further investigated by TEM. A selected area electron diffraction (SAED) pattern of a plan-view sample is shown in figure 1(b). In the lower right part of the electron diffraction pattern, simulated rings corresponding to a (0002)-textured hcp phase are superimposed on the experimental pattern (using values  $a = 2.61 \text{ \AA}$  and  $c = 4.24 \text{ \AA}$  deduced from the SAED pattern and from XRD, respectively). In the same way, in the upper right part of figure 1(b), simulated rings for a (111)-

textured fcc phase (bulk value  $a = 3.675 \text{ \AA}$ ) are shown. These simulations indicate that the diffraction rings 2, 5, and 6a can be indexed both as (11-20), (3-300) and (22-40) reflections of the (0002)-textured hcp phase or as the (220), (224) and (440) reflections of the (111)-textured fcc phase. In contrast, the positions of the (1a: 1-100), (3a: 2-200), (4a: 12-30), and (6b: 31-40) rings are exclusively characteristic of the (0002)-textured hcp phase. Other weak rings (1b and 3b) refer either to the (111) and (113) fcc reflections, or to the (0002) and (11-22) reflections of the hcp phase but not to CoO. Please note, that these rings are neither expected for the (0002)-textured hcp phase nor for the (111)-textured fcc phase, indicating that a small amount of crystallites has different orientations. From the SAED pattern, no conclusive picture about the occurrence of an additional fcc phase can be drawn. However, high resolution images of the Co<sub>3</sub>Pt layer indicate the existence of fcc grains similar to earlier observations [28]. Nevertheless, the high intensity of the (1-100) ring suggests a strong (0002)-textured hcp phase in the Co<sub>3</sub>Pt film. Moreover, it has been checked, that the weak reflections do not originate from CoO.

By analysis of the cross-section TEM images (figure 2), the thickness of the Co<sub>3</sub>Pt layer was estimated to be  $(4.8 \pm 0.3) \text{ nm}$  whereas the lateral size of the Co<sub>3</sub>Pt grains is in the order of 20 nm. However, within one grain, there might be a number of small-angle boundaries. Besides this, areas with smaller Co<sub>3</sub>Pt grains of about 2 nm were found (not shown). Furthermore, a tilt of the *c*-axis of the grains of up to 10° from the film normal was observed (figure 2(b, c)), which is in agreement with the broad rocking curve (figure 1(a)). Please note that the observed canting of the *c*-axis has important consequences on the magnetic properties of the Co<sub>3</sub>Pt alloy film as discussed later.

In the CoO layer, small grains with a typical size below 3 nm were found. However, also a few larger grains with sizes of more than 5 nm were observed. The thickness of the CoO layer could not be determined, since there is no clear separation between CoO and the epoxy adhesive used for TEM sample preparation, but an estimation with the densities and molar masses of Co and CoO leads to a CoO thickness of at least 1.7 nm from the deposition of the additional Co layer.

An AFM study was carried out to access the overall surface morphology. The study revealed a root mean square (rms) roughness of the single Co<sub>3</sub>Pt layer of about 0.3 nm. With the addition of the CoO layer an increase of the rms roughness to about 0.5 nm was observed.

### **Magnetic characterization**

The saturation magnetization,  $M_s$ , of the Co<sub>3</sub>Pt film was estimated from SQUID measurements to be  $(900 \pm 140) \text{ emu/cm}^3$  which is slightly lower compared to the bulk value of  $1100 \text{ emu/cm}^3$  [29, 30]. The OOP

loop (figure 3) shows a sharp switching behaviour at a field of  $H_C = 525$  Oe and a remanent magnetization of about  $0.85 \cdot M_S$ ; whereas the IP loop displays characteristic hard axis behaviour. The presence of a perpendicular easy axis of magnetization is in agreement with earlier works reported by Yamada et al. [31, 32]. Based on our structural study, the PMA is caused by the growth of hcp  $\text{Co}_3\text{Pt}$  grains with their  $c$ -axes pointing preferentially in OOP direction. Please note that a high magnetic field of about 40 kOe is necessary to completely saturate the layer in OOP geometry (figure 3) which is likely caused by the canting of the  $c$ -axes of the  $\text{Co}_3\text{Pt}$  grains (figure 2(c)). Thus, the reversal in the high field region reflects a rotation away from the canted  $c$ -axis towards the field direction.

### (A) Exchange bias field in OOP and IP direction

The magnetic hysteresis of a  $\text{Co}_3\text{Pt}$  layer with an oxidized 1-nm-thick Co film is seen in figure 4. The additional CoO layer leads to a reduction of the OOP remanent magnetization and to an increase of the remanence in IP direction when compared to the  $\text{Co}_3\text{Pt}$  single layer (figure 4(a, c)). The reduction of the OOP remanence might be related to the modification of the surface anisotropy of the  $\text{Co}_3\text{Pt}$  film triggered by the deposition of the crystalline Co capping layer, as it was recently reported by Shipton et al. [25] for exchange biased  $\text{CoO}/[\text{Co}/\text{Pt}]$  films. Furthermore, the addition of the AF layer leads to a substantial enhancement of the coercivity in both OOP and IP directions.

The hysteresis loop measured at  $T_{\text{meas}} = 10$  K on the  $\text{CoO}/\text{Co}_3\text{Pt}$  film shows an exchange bias field of about 340 Oe after field cooling in 70 kOe in both OOP and IP geometries (figure 4(b, d)). Note that also for the single  $\text{Co}_3\text{Pt}$  layer a comparatively small exchange bias effect ( $H_{\text{EB}} < 50$  Oe) with a blocking temperature,  $T_B$ , of about 30 K was observed. It can be concluded that the natural oxidation of the single  $\text{Co}_3\text{Pt}$  layer forms only a marginal amount of AF CoO likely due to the surface segregation of Pt during co-deposition resulting in a partial passivation of the surface. Figure 5 summarizes the EB and coercive fields as a function of  $T_{\text{meas}}$  in both measurement geometries (OOP and IP) for  $\text{CoO}/\text{Co}_3\text{Pt}$  in comparison with single  $\text{Co}_3\text{Pt}$  layers.

Above 150 K the exchange bias field becomes zero, suggesting an upper limit for the blocking temperature  $T_B$  of the same order. With decreasing measurement temperature, the EB field measured on  $\text{CoO}/\text{Co}_3\text{Pt}$  gradually increases down to 10 K indicating that some AF grains are still thermally unstable at this temperature. CoO is a rather strong AF with an anisotropy constant,  $K_{\text{AF}}$ , of  $29 \times 10^7$  ergs/cm<sup>3</sup> [33]. However, the mean size of the CoO grains of about 3 nm leads to a reduced thermal stability of the AF grains [12, 34]. In this respect, only AF grains with high magnetic anisotropy energy, which are stable at  $T_{\text{meas}}$ , can contribute

to EB. Following the model by O'Grady et al. [12] which accounts for a size distribution of the AF grains, the temperature dependence of  $H_{EB}$  in OOP geometry was measured (figure 6(a)) and its derivative was fitted with a log-normal peak function (figure 6(b)). The area under the curve includes all AF grains that are stable and thus allows to extract the maximum exchange bias field,  $H_{EB,max}$ . With this method we found  $H_{EB,max} = 433$  Oe. Using this value, the exchange energy at the AF/F interface was calculated to be  $J_{EB,OOP} = M_S \cdot H_{EB,max} \cdot t_{FM} = 0.19$  ergs/cm<sup>2</sup>. The value of  $J_{EB,OOP}$  is lower than the interfacial exchange energy of 0.25 ergs/cm<sup>2</sup> reported for CoO/[Co/Pt] [20]. Furthermore, in the CoO/Co<sub>3</sub>Pt system the interfacial exchange coupling energy in OOP and IP direction is found to be the same within the margin of error ( $J_{EB,IP}/J_{EB,OOP} \approx 1$ ) in agreement with the expected isotropy of the orientation of the easy axes in the grains of the polycrystalline AF film. In contrast to this finding, a value of  $J_{EB,IP}/J_{EB,OOP} \approx 2$  was obtained for CoO/[Co/Pt] [20]. The smaller interfacial exchange energy measured in IP direction for CoO/Co<sub>3</sub>Pt compared to CoO/[Co/Pt] indicates that a smaller amount of AF grains have their easy axes close to the IP cooling direction, as required for IP exchange bias [20]. The latter might be attributed to the different crystalline quality of F grains in the two systems. Indeed, in contrast to the room temperature growth of the Co<sub>3</sub>Pt alloy, the deposition of Co/Pt multilayers was carried out at an elevated temperature of 420 K [20], which might result in larger CoO grains with improved texture. This assumption is supported by the observed difference in blocking temperature (220 K for CoO/[Co/Pt] and 100 K for CoO/Co<sub>3</sub>Pt), which is related to the anisotropy energy of the AF layer and thus to the AF grain size.

## (B) Coercive field dependence

The temperature dependence of the coercivity caused by the EB effect is one of the least understood phenomena in EB. A recent review of the existing theoretical models is given by O'Grady et al. [12].

Figure 6(c) displays the difference,  $\Delta H_C$ , between the coercivities of the Co<sub>3</sub>Pt films with and without CoO in OOP geometry. The temperature dependence of  $\Delta H_C$  was fitted with a log-normal peak function subtracting an exponential background (figure 6(c), dashed line). Please note that even at temperatures higher than  $T_B$ , the difference in  $H_C$  does not vanish and remains at about 75 Oe. This might be related to the modification of the interface properties between the Co<sub>3</sub>Pt and CoO layers which will affect the distribution of nucleation/pinning sites. However, an influence of the paramagnetic CoO due to fluctuations of magnetic moments on the magnetization reversal behaviour of the F layer might also contribute to the coercive field of the CoO/Co<sub>3</sub>Pt bilayer. A similar idea was applied by Cai et al. [35] to explain the influence of an AF layer with  $T_N > T_C$  on a ferromagnetic film above its Curie temperature.

With decreasing measurement temperature  $T_{\text{meas}}$ , the difference in the coercive field of the  $\text{Co}_3\text{Pt}$  film with and without CoO layer is found to become more pronounced (figure 6(c)). According to Stiles and McMichael [5, 6], there are two possible mechanisms for increased coercivity in EB bilayer systems assuming a polycrystalline microstructure of the AF: (i) inhomogeneous reversal in the ferromagnet and (ii) irreversible switching of the antiferromagnetic order in AF grains as they follow the F magnetization due to interfacial coupling. The first mechanism is caused by spatially inhomogeneous coupling of the F to the uncompensated frozen AF spins which contributes at all temperatures below  $T_B$ : With the decrease of  $T_{\text{meas}}$  the contribution of this mechanism becomes more pronounced as more grains get frozen during the cooling procedure and the interfacial exchange area increases. Therefore, the observed gradual increase in  $\Delta H_C(T_{\text{meas}})$  (figure 6(c), dashed line) can be attributed to the increasing number of frozen uncompensated spins. As these are also responsible for the shift of the hysteresis loop (EB field), the background adopts the same functional dependency on  $T_{\text{meas}}$  as the exchange bias field, which was approximated by an exponential decay.

In contrast, the contribution from irreversible switching of AF spins is expected to be weak at low temperatures having the strongest impact in the vicinity of the blocking temperature of the AF, where the anisotropy of the AF grains becomes largest before ceasing to be rotatable by the reversal of the F layer [5, 6]. Thus, the non-monotonic dependence of  $\Delta H_C(T_{\text{meas}})$  is a result of AF spins, which are stable in zero field at  $T_{\text{meas}}$ , but can switch irreversibly following the orientation of the magnetic moment of the F layer, when driving the field from positive to negative saturation. These AF spins are called rotatable spins which give rise to an additional energy barrier that needs to be overcome for the magnetic reversal process and, thus, lead to an increase of the coercive field of the coupled AF/F layers. Such non-monotonic  $H_C(T_{\text{meas}})$  behaviour was observed in soft magnetic layers exchange biased by CoO [14, 36] and in  $\text{CoO}/[\text{Co}/\text{Pd}]$  films with OOP easy axis of magnetization [21]. By subtracting the background due to the inhomogeneous F reversal (figure 6(c), dashed line), we are left with the contribution of irreversible switching of AF spins to the coercive field of the F layer. Please note that the resulting  $\Delta H_C(T_{\text{meas}})$  dependence should resemble the AF grain size distribution (fraction of AF grains becoming thermally stable at  $T_{\text{meas}}$ ) and was thus fitted using a log-normal peak function (figure 6(c)). Indeed, for a given temperature  $T_{\text{meas}}$ , only spins in AF grains, which have their thermal destabilization temperature just above  $T_{\text{meas}}$ , are subject to such switching and exhibit rotatable anisotropy. In contrast, spins in larger (more stable) AF grains will not switch and thus can contribute to unidirectional anisotropy resulting in a shift of a hysteresis loop. The limit at which the anisotropy changes from rotatable to unidirectional is defined by the coupling strength. AF spins coupled to the F layer with the

exchange energy  $J_{EB}$  can be reversed if their anisotropy energy,  $K_{AF} \cdot t_{AF}$  ( $t_{AF}$  is the thickness of the AF layer), can be overcome by the coupling energy. Usually the anisotropy energy is much larger than the exchange coupling energy, but the energy barrier is reduced by the aid of the thermal energy. If the energy barrier can be easily overcome at high temperatures, AF grains are not stable and behave paramagnetically contributing to neither  $H_{EB}$  nor  $H_C$ . Due to the different stability requirements for unidirectional and rotatable anisotropy, the peak in the derivative of  $H_{EB}$  occurs at a lower temperature than the one in the  $\Delta H_C(T_{meas})$  dependence (figure 6) as the frozen state is reached later than the rotatable state during cooling.

Please note that in IP geometry the investigation of the EB related coercivity enhancement was not carried out due to the presence of an in-plane anisotropy caused by the CoO layer, which is the main source for the increased coercivity.

### (C) Cooling field study

A strong cooling field dependence of both the exchange bias field and coercivity is typically observed for exchange bias systems [4, 12, 21, 37].

As can be seen from figure 7(a), no difference in the OOP hysteresis loops was observed for the CoO/Co<sub>3</sub>Pt film even when a reverse cooling field (smaller than coercive field at room temperature) was applied to the initially saturated sample. However, the sign of  $H_{EB}$  was changed when the reverse cooling field exceeded the coercive field at room temperature (not shown). This observation suggests that the stray field provided by the Co<sub>3</sub>Pt film at remanence (about 10 kOe) is already sufficient to align the CoO spins when cooled through  $T_N$ .

In this respect, it is interesting to note that due to the relatively small IP remanent magnetization, the setting of the AF layer at remanence in IP geometry is not efficient compared to the OOP case. Therefore, a pronounced cooling field dependence of the exchange bias field was observed (figure 7(b)). In this case  $H_{EB,IP}(H_{cool})$  is correlated with the strength of the IP magnetization at room temperature thus following the room temperature IP hysteresis loop (figure 4(c)).

It is important to note that the coercive field,  $H_C$ , reveals no cooling field dependence in both OOP and IP geometries (not shown) because the F layer in the studied system provides a sufficient magnetic field while cooling through the Néel temperature to align the spins in the thin AF layer with respect to the local orientation of the F spins. As the F spins reverse during the measurement of a hysteresis loop, the torque provided by the magnetization of the F layer will switch the rotatable AF spins without regards to their initial state after cooling. This means that the exhibited rotatable anisotropy is not bound to a specific cooling

configuration in the AF which is in agreement with the theory by Stiles and McMichael [4]. Therefore, even if the mean unidirectional anisotropy induced by the cooling procedure varies (figure 7(b), IP curve), the rotatable anisotropy does not change, resulting in constant  $H_C$  of the obtained loops.

## Summary

We presented a study on the exchange bias effect in hcp (0002)-textured  $\text{Co}_3\text{Pt}$  alloy films coupled to a thin antiferromagnetic CoO layer. The  $\text{Co}_3\text{Pt}$  layer shows an out-of-plane easy axis of magnetization. The model of grainy polycrystalline AF was applied to interpret the obtained experimental data on the magnetic properties of the samples. It was shown that in contrast to previous observations on perpendicular CoO/[Co/Pt] systems, CoO/ $\text{Co}_3\text{Pt}$  reveals similar exchange bias fields in OOP and IP geometry for maximum cooling fields, i.e. when the F layer is fully saturated. This is attributed to the different quality of the AF/F interface.

Furthermore, the dependence of the coercivity enhancement due to the EB effect was investigated by comparing identical F films with and without CoO. It was found that there are two contributions to the enhancement of the coercive field in perpendicular CoO/ $\text{Co}_3\text{Pt}$  systems, which can be identified following the theory developed by Stiles and McMichael as inhomogeneous reversal in the F film and irreversible switching of AF spins. While the first mechanism has the same origin as the loop shift (uncompensated frozen spins), the other one is related to the rotatable anisotropy characteristic of partially stable AF spins which are just below their destabilization temperature. Furthermore, the difference in the temperature evolution of the coercive field given by rotatable spins and the exchange bias field given by frozen spins indicates that AF grains undergo two transitions during the cooling process: First, from the paramagnetic state to the state exhibiting rotatable anisotropy and second, to the frozen state. The transition behaviour can be accessed by measuring the temperature evolutions of  $\Delta H_C$  and  $dH_{EB}/dT_{\text{meas}}$ .

Interestingly, the CoO/ $\text{Co}_3\text{Pt}$  samples did not reveal a cooling field dependence of the exchange bias field when initially saturated in OOP direction. It is assumed that the high remanence magnetization of the  $\text{Co}_3\text{Pt}$  film results in a strong stray field at the AF/F interface leading to a setting of the AF layer even without an applied magnetic field. In contrast, in IP direction the exchange bias field is correlated with the strength of the IP magnetization at room temperature thus following the room temperature hysteresis loop of the  $\text{Co}_3\text{Pt}$  film. The coercive field was not dependent on the cooling configuration for both OOP and IP geometries.

## **Acknowledgement**

We would like to thank Dr. F. Radu (HZB, Berlin) and C. Brombacher for fruitful discussions, Prof. R. Magerle for the opportunity to perform AFM studies, P. Matthes for assistance in AFM measurements, and G. Baumann for TEM sample preparation. Part of this research was carried out at the light source HASYLAB (beamline G3) at DESY (Hamburg) and the financial support (project No. I-20090119) is gratefully acknowledged. In addition, H.S. acknowledges financial support through the Landesinnovationspromotion (financed by Free State of Saxony and European Social Fund).

## Figure Captions

Fig. 1: (a) XRD  $\theta$ - $2\theta$  pattern and rocking curve (RC) of the 5-nm-thick Co<sub>3</sub>Pt film. (b) SAED pattern of a plan-view sample. The calculated rings corresponding to the (111) fcc and (0002) hcp textured phases are drawn in the upper and lower right parts, respectively. The bright spots on the left and right sides come from the Si(100) substrate.

Fig. 2: (a) Cross-sectional TEM image of the CoO/Co<sub>3</sub>Pt sample. The lower panels show high resolution images taken of different Co<sub>3</sub>Pt grains: (b) lattice planes are almost parallel to the substrate plane (out-of-plane  $c$ -axis); (c) lattice planes are approximately 10° tilted with respect to the substrate plane (canted  $c$ -axis). Lattice contrast in panels (b) and (c) has been enhanced by Fourier-filtering and standard image processing techniques which led to delocalized lattice fringes in the amorphous adhesive used for sample preparation in the top left corners.

Fig. 3: Out-of-plane and in-plane SQUID hysteresis loops of the single Co<sub>3</sub>Pt film measured at 300 K. The inset shows a zoomed region of the loops around the zero field axis.

Fig. 4: SQUID hysteresis loops of the Co<sub>3</sub>Pt samples without (open symbols) and with (solid symbols) CoO layer. Panels (a) and (c) show loops measured at  $T_{\text{meas}} = 300$  K; panels (b) and (d) show loops measured at  $T_{\text{meas}} = 10$  K after field cooling in  $H_{\text{cool}} = 70$  kOe. Please note the difference in the shown field range of this figure compared to Fig. 3, hiding the further increase of the OOP magnetization with increasing magnetic field.

Fig. 5: Temperature dependence of the exchange bias field,  $H_{\text{EB}}$ , and coercivity,  $H_{\text{C}}$ , in (a) out-of-plane and (b) in-plane geometry after field cooling in  $H_{\text{cool}} = 70$  kOe.

Fig. 6: (a) Temperature dependence of the OOP EB field. (b) Log-normal peak function fit of  $dH_{\text{EB}}/dT_{\text{meas}}$ . (c) Difference between the OOP coercive fields of the Co<sub>3</sub>Pt alloy films with and without CoO layer.

Fig. 7: (a) Out-of-plane SQUID hysteresis loops of the CoO/Co<sub>3</sub>Pt stack measured at 10 K after field cooling in various  $H_{\text{cool}}$ . The image shows 5 hysteresis loops for cooling fields of  $H_{\text{cool}} = +70, +5, +0.4, 0, -0.4$  kOe ( $H_{\text{C}}$  of Co<sub>3</sub>Pt at 300 K is -0.5 kOe). (b) Cooling field dependence of the EB fields in IP and OOP direction. The data is extracted from the hysteresis loops taken at  $T_{\text{meas}} = 10$  K in IP and OOP geometry after cooling in a field  $H_{\text{cool}}$ .

## References

- [1] Meiklejohn W H and Bean C P 1956 *Phys. Rev.* **102**, 1413
- [2] Berkowitz A E and Takano K 1999 *J. Magn. Magn. Mater.* **200**, 552
- [3] Nogués J and Schuller I K 1999 *J. Magn. Magn. Mater.* **192**, 203
- [4] Radu F and Zabel H 2007 *Springer Tracts Mod. Phys.* **227**, 97
- [5] Stiles M D and McMichael R D 1999 *Phys. Rev. B* **60**, 12950
- [6] Stiles M D and McMichael R D 2001 *Phys. Rev. B* **63**, 064405
- [7] Malozemoff A P 1987 *Phys. Rev. B* **35**, 3679
- [8] Mauri D, Siegmann H C, Bagus P S and Kay E 1987 *J. Appl. Phys.* **62**, 3047
- [9] Nowak U, Usadel K D, Keller J, Miltényi P, Beschoten B and Güntherodt G 2002 *Phys. Rev. B* **66**, 014430
- [10] Suess D, Kirschner M, Schrefl T, Fidler J, Stamps R L and Kim J-V 2003 *Phys. Rev. B* **67**, 054419
- [11] Nogués J, Sort J, Langlais V, Skumryev V, Suriñach S, Muñoz J S and Baró M D 2005 *Phys. Rep.* **422**, 65
- [12] O'Grady K, Fernandez-Outon L E and Vallejo-Fernandez G 2010 *J. Magn. Magn. Mater.* **322**, 883
- [13] Radu F, Mishra S K, Zizak I, Erko A I, Dürr H A, Eberhardt W, Nowak G, Buschhorn S, Zabel H, Zhernenkov K, Wolff M, Schmitz D, Schierle E, Dudzik E and Feyerherm F 2009 *Phys. Rev. B* **79**, 184425
- [14] Berkowitz A E, Hong J-I, McCall S K, Shipton E, Chan K T, Leo T and Smith D J 2010 *Phys. Rev. B* **81**, 134404
- [15] Rottmayer R and Zhu J-G 1995 *IEEE Trans. Magn.* **31**, 2597
- [16] Moodera J S, Kinder L R, Wong T M and Meservey R 1995 *Phys. Rev. Lett.* **74**, 3273 (1995).
- [17] Dieny B, Humbert P, Speriosu V S, Metin S, Gurney B A, Baumgart P, and Lefakis H 1992 *Phys. Rev. B* **45**, 806
- [18] Ludwig K, Hauch J, Mattheis R, Barholz K-U and Rieger G 2003 *Sens. Actuators A* **106**, 15
- [19] Lamberton R, Seigler M, Pelhos K, Zhou H, McCurry M, Ormston M, Yi G, McClean G, McLaughlin T, Kolbo P, Heininen O, Sapozhnikov V and Mao S 2007 *IEEE Trans. Magn.* **43**, 645
- [20] Maat S, Takano K, Parkin S S P and Fullerton E E 2001 *Phys. Rev. Lett.* **87**, 087202
- [21] Guhr I L, Hellwig O, Brombacher C and Albrecht M 2007 *Phys. Rev. B* **76**, 064434
- [22] Guhr I L, van Dijken S, Malinowski G, Fischer P, Springer F, Hellwig O and Albrecht M 2007 *J. Phys. D: Appl. Phys.* **40**, 3005
- [23] Malinowski G, Albrecht M, Guhr I L, Coey J M D and van Dijken S 2007 *Phys. Rev. B* **75**, 012413
- [24] Baruth A and Adenwalla S 2010 *J. Magn. Magn. Mater.* **322**, 2051

- [25] Shipton E, Chan K, Hauet T, Hellwig O and Fullerton E E 2009 *Appl. Phys. Lett.* **95**, 132509
- [26] Dahmani C E 1985 PhD thesis, Louis Pasteur University Strasbourg.
- [27] Harp G R, Weller D, Rabedeau T A, Farrow R F C and Toney M F 1993 *Phys. Rev. Lett.* **71**, 2493
- [28] Maret M, Ulhaq-Bouillet C, Staiger W, Cadeville M C, Lefebvre S and Bessière M 1998 *Thin Solid Films* **319**, 191
- [29] Maret M, Cadeville M C, Herr A, Poinot R, Beaurepaire E, Lefebvre S and Bessière M 1999 *J. Magn. Magn. Mater.* **191**, 61
- [30] Bolzoni F, Leccabue F, Panizzieri R and Pareti L 1984 *IEEE Trans. Magn.* **20**, 1625
- [31] Yamada Y, Suzuki T and Abarra E N 1997 *IEEE Trans. Magn.* **33**, 3622
- [32] Yamada Y, Van Drent W P, Abarra E N and Suzuki T 1998 *J. Appl. Phys.* **83**, 6527
- [33] Kanamori J 1957 *Prog. Theor. Phys.* **17**, 177, **17**, 197
- [34] Choo D, Chantrell R W, Lamberton R, Johnston A and O'Grady K 2007 *J. Appl. Phys.* **101**, 09E521
- [35] Cai J W, Liu K and Chien C L 1999 *Phys Rev. B* **60**, 72
- [36] Gurgul J, Freindl K, Koziół-Rachwał A, Matlak K, Spiridis N, Ślęzak T, Wilgocka- Ślęzak D and Korecki J 2010 *Surf. Interface Anal.* **42**, 696
- [37] Ambrose T and Chien C L 1998 *J. Appl. Phys.* **83**, 7222

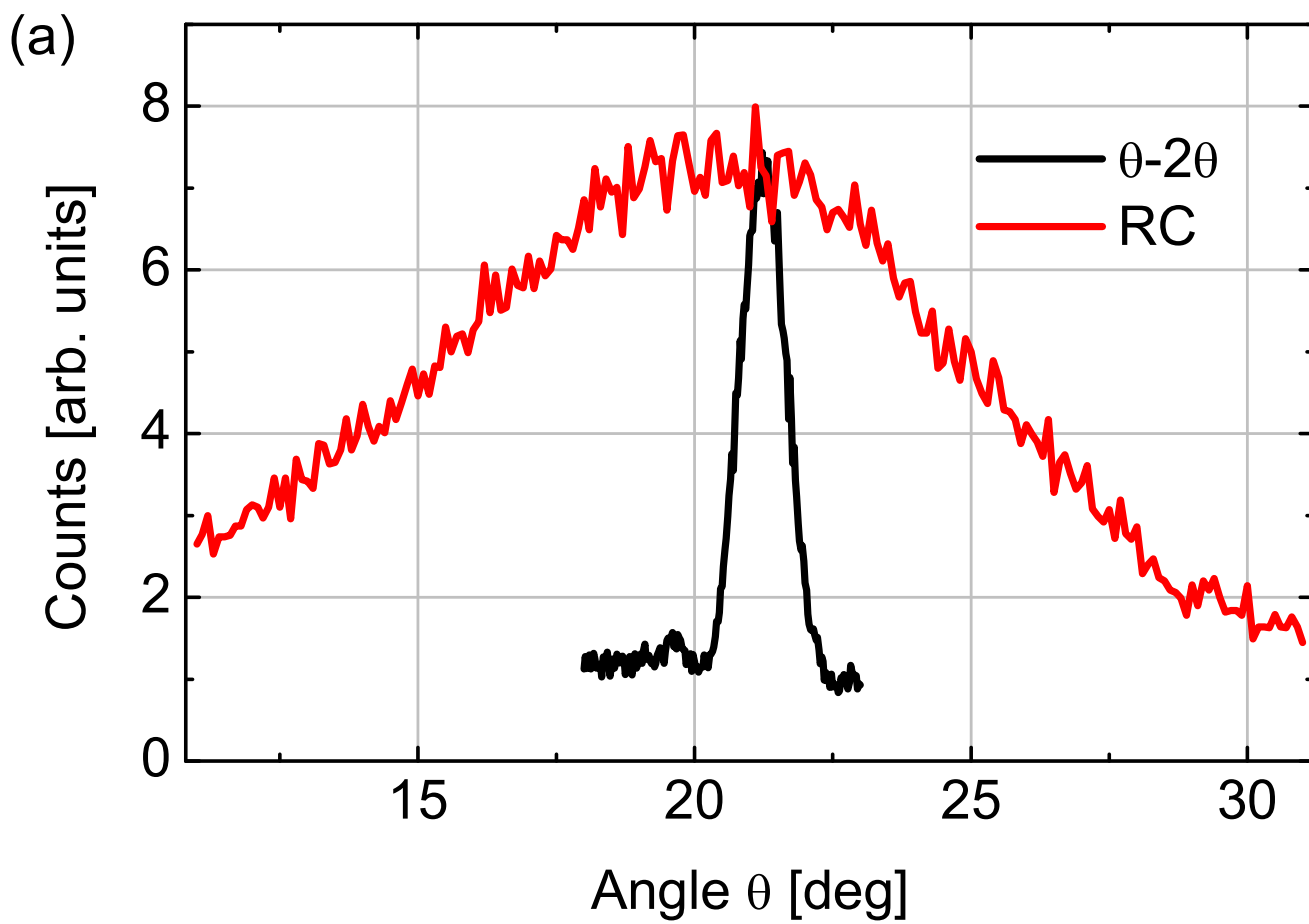


Figure 1a (revision/figure1a.eps)

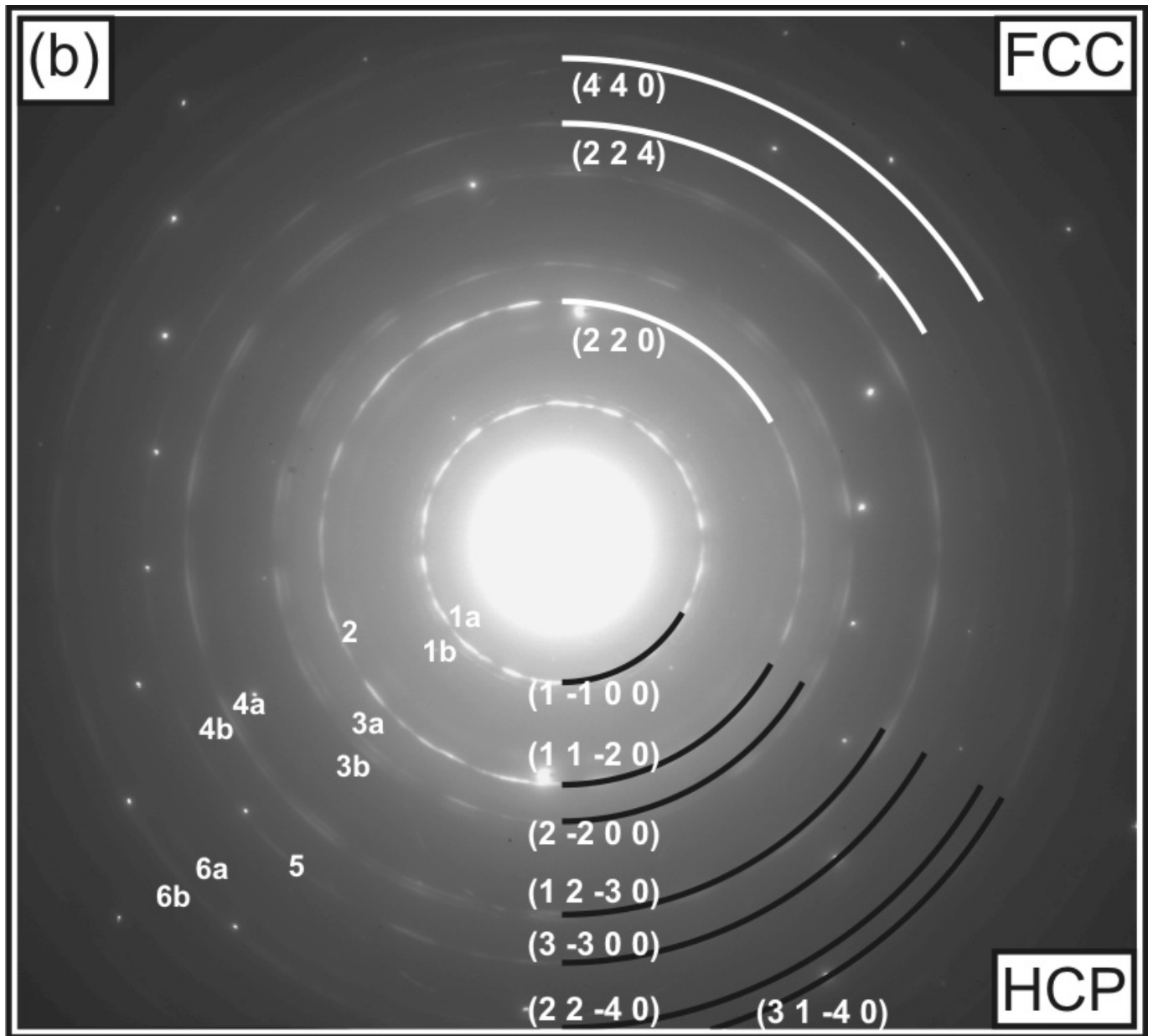


Figure 1b (revision/figure1b.jpg)

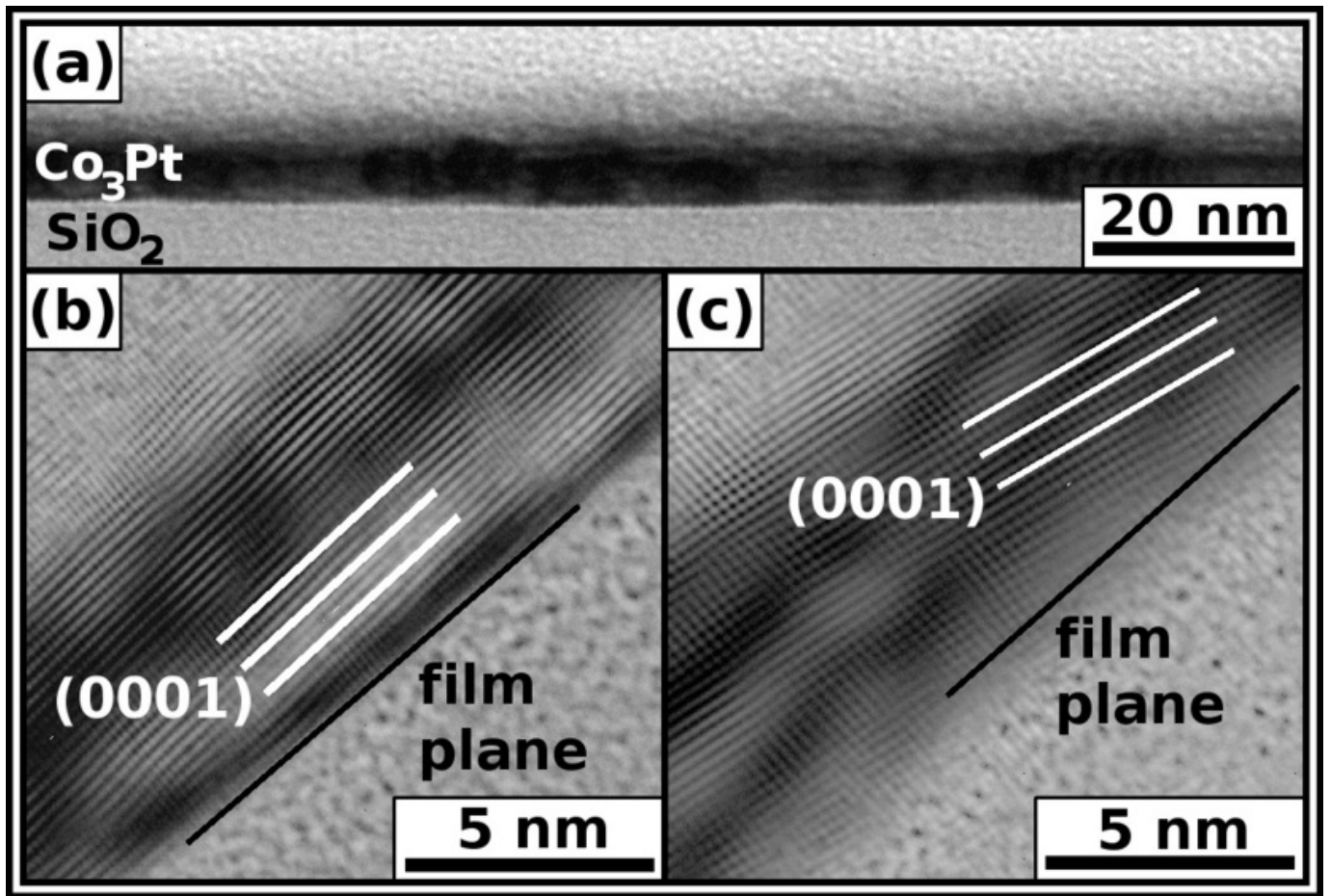


Figure 2abc (revision/figure2a\_2c.jpg)

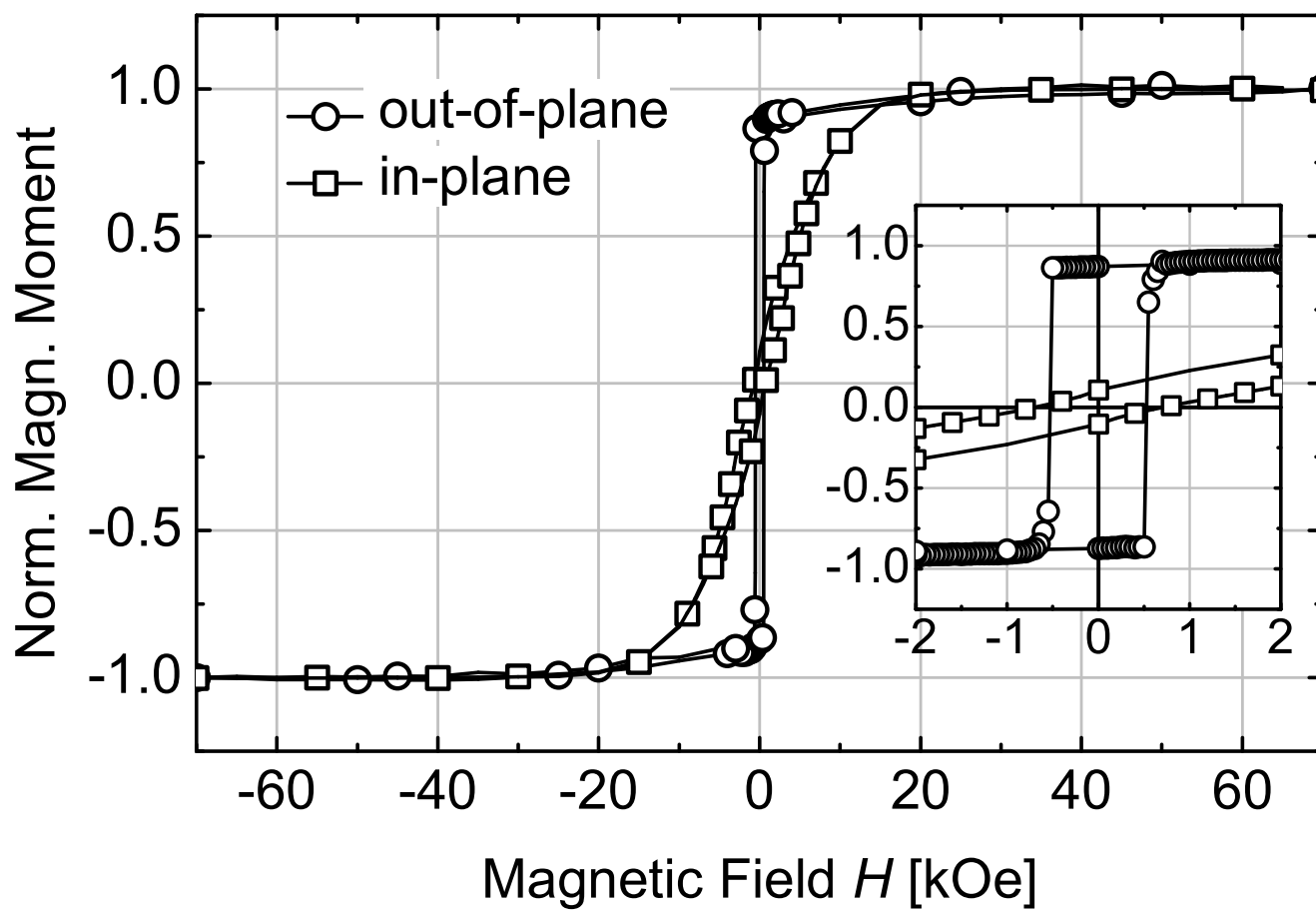


Figure 3 (revision/figure3.eps)

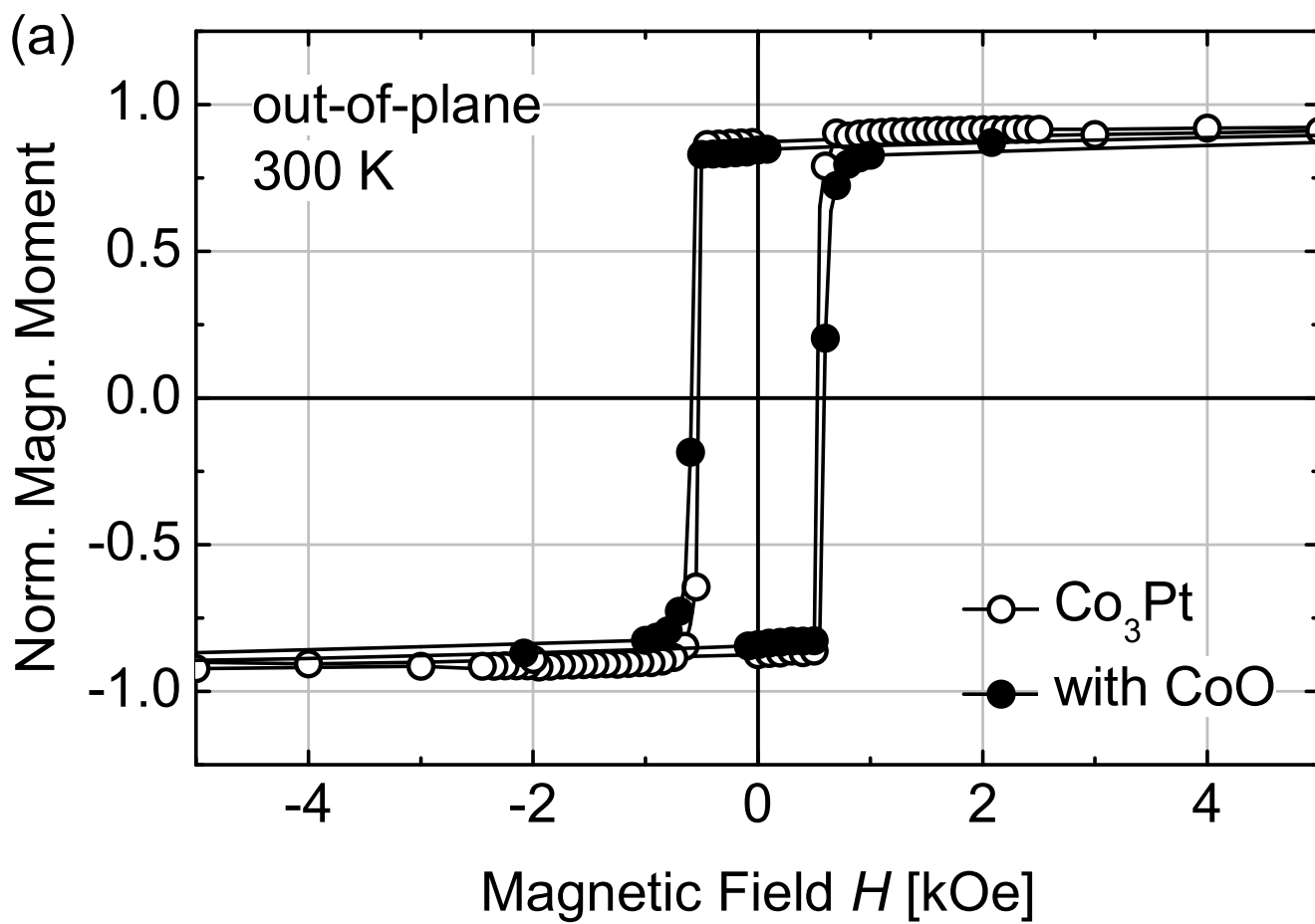


Figure 4a (revision/figure4a.eps)

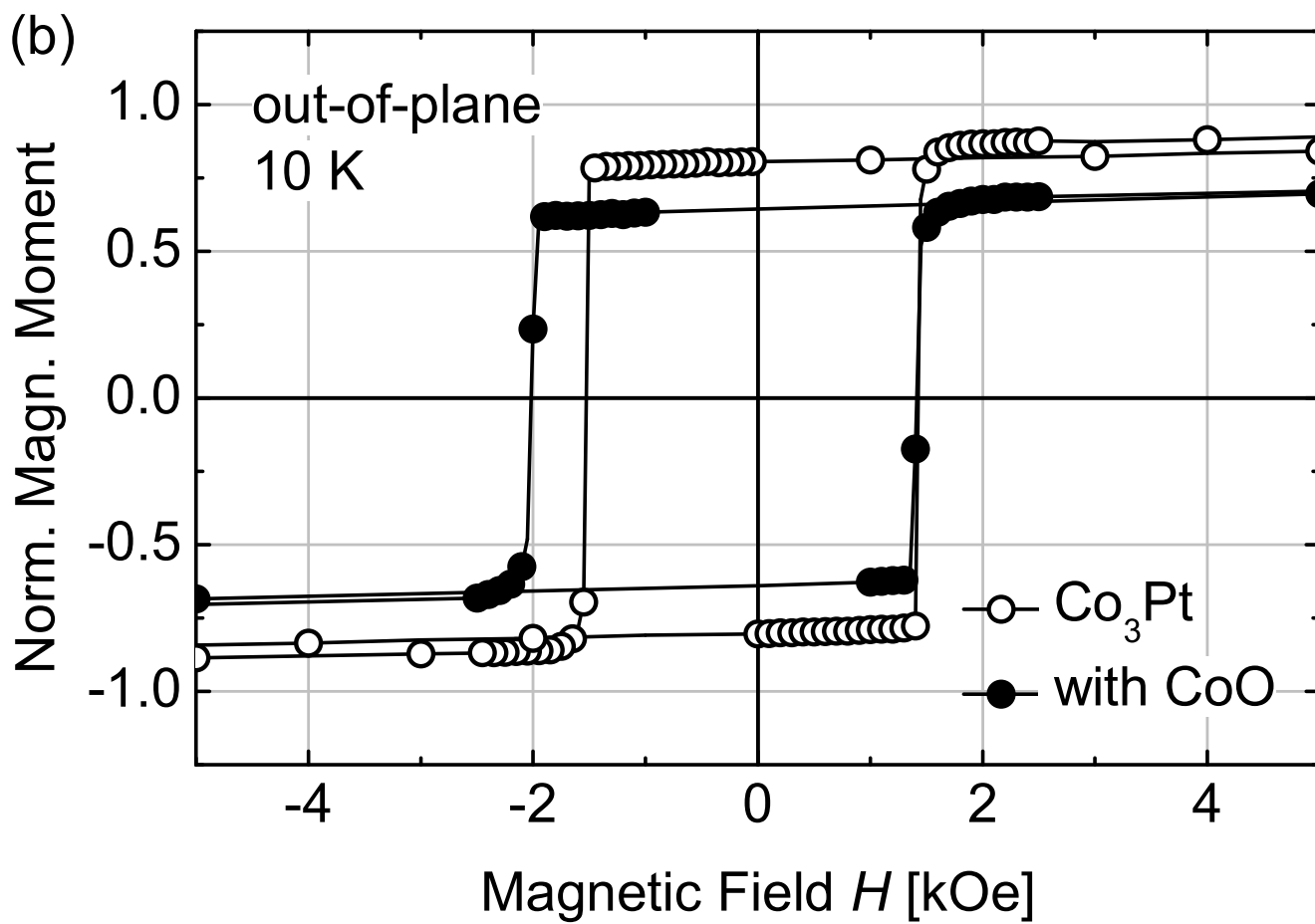


Figure 4b (revision/figure4b.eps)

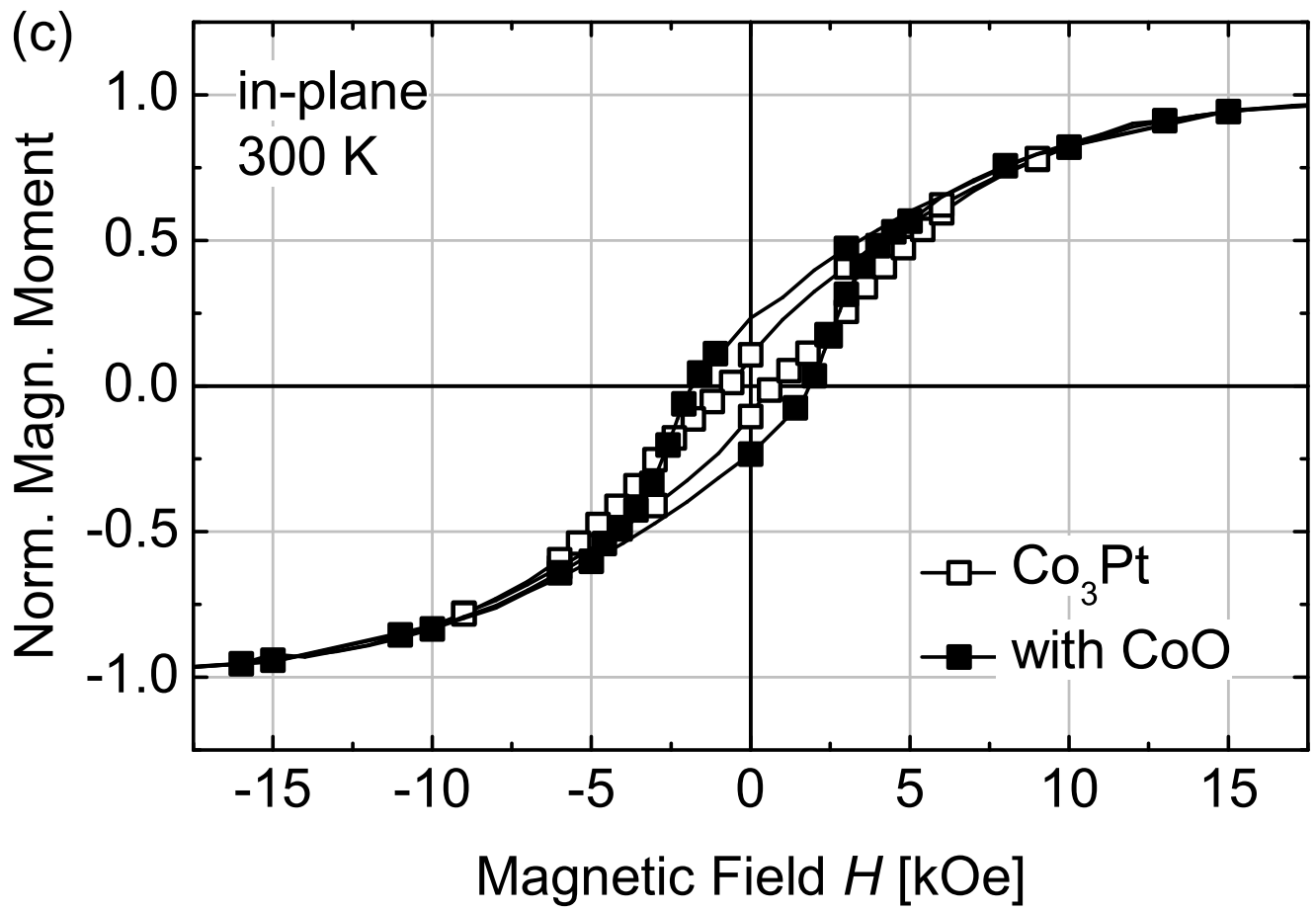


Figure 4c (revision/figure4c.eps)

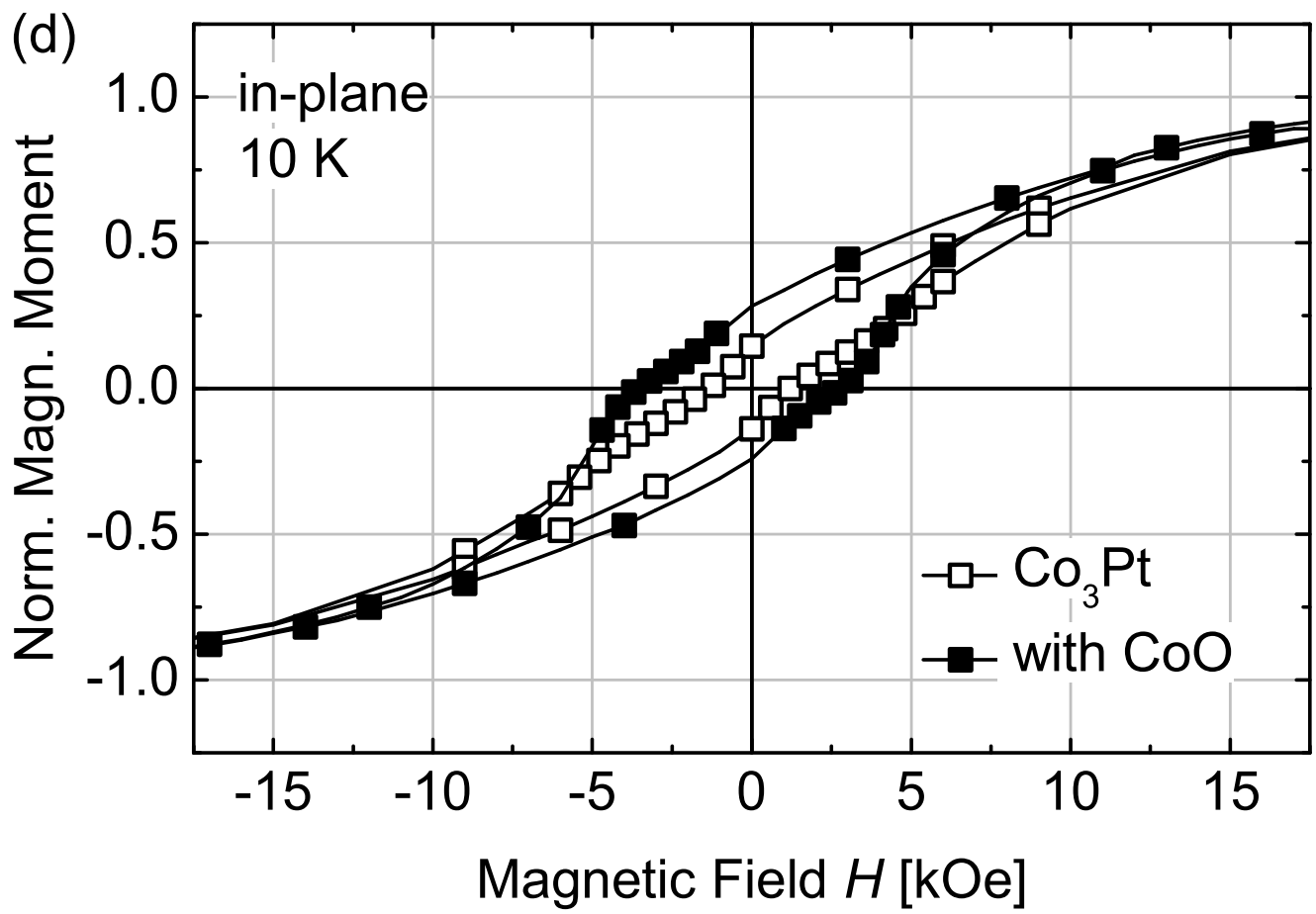


Figure 4d (revision/figure4d.eps)

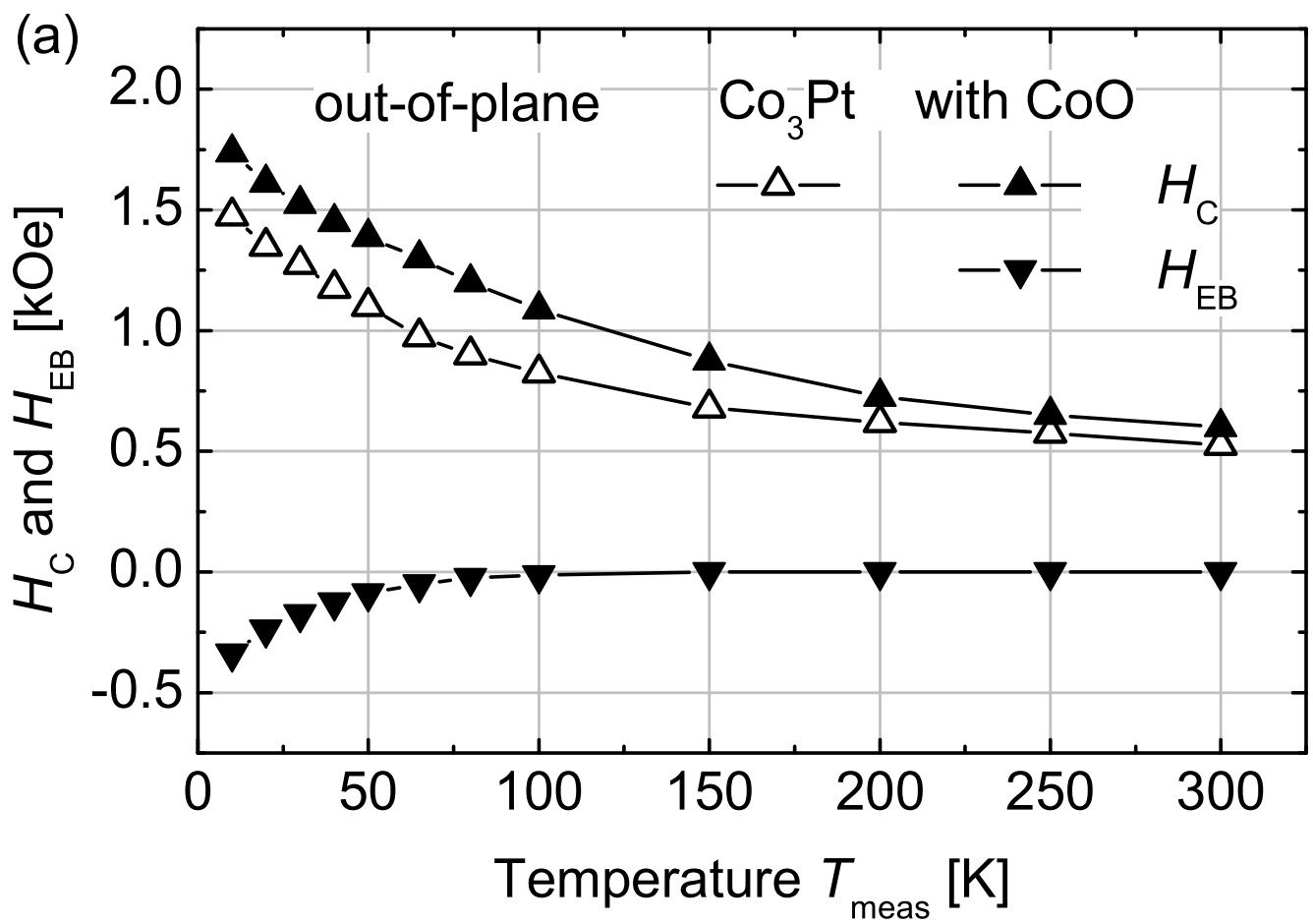


Figure 5a (revision/figure5a.eps)

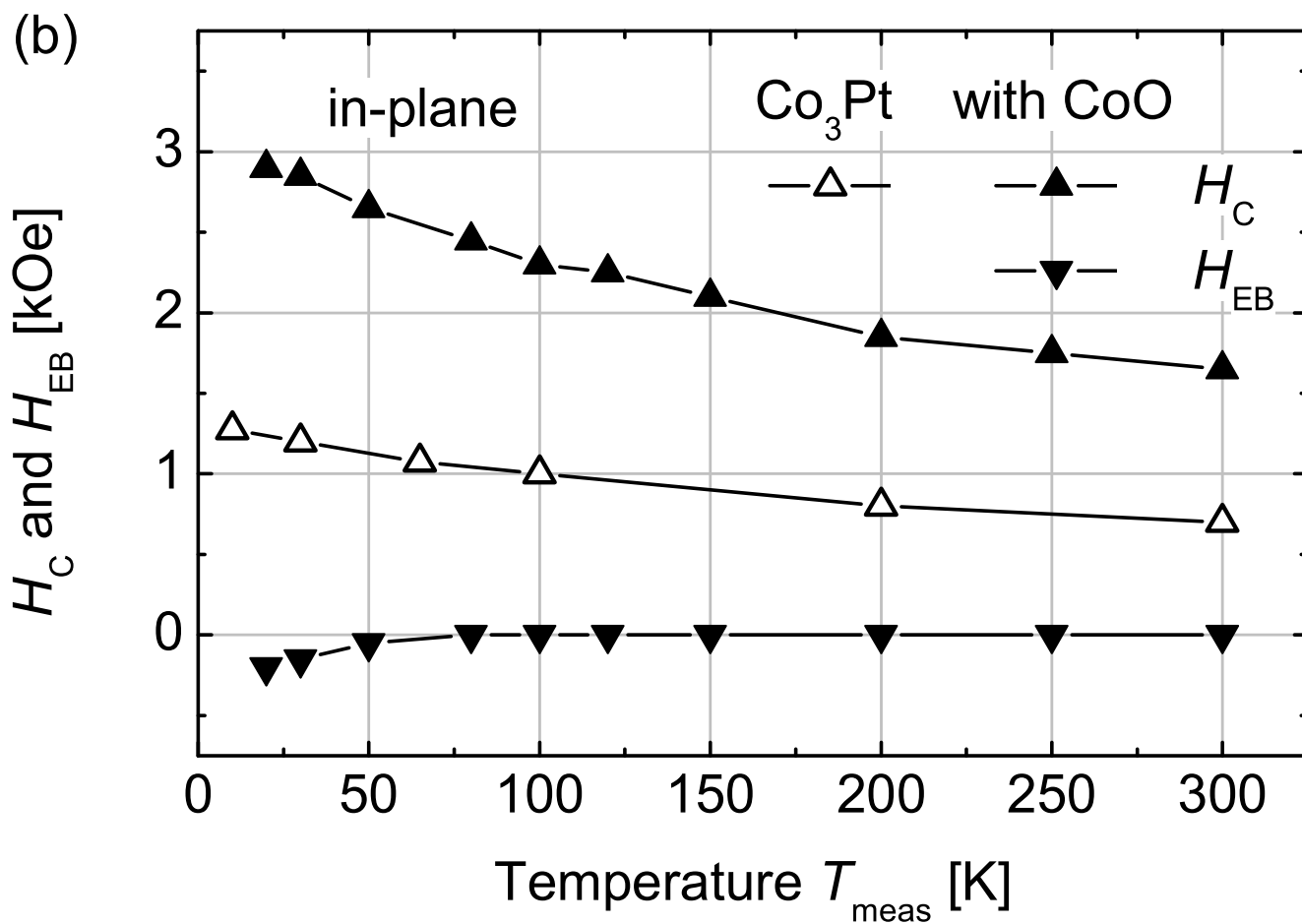


Figure 5b (revision/figure5b.eps)

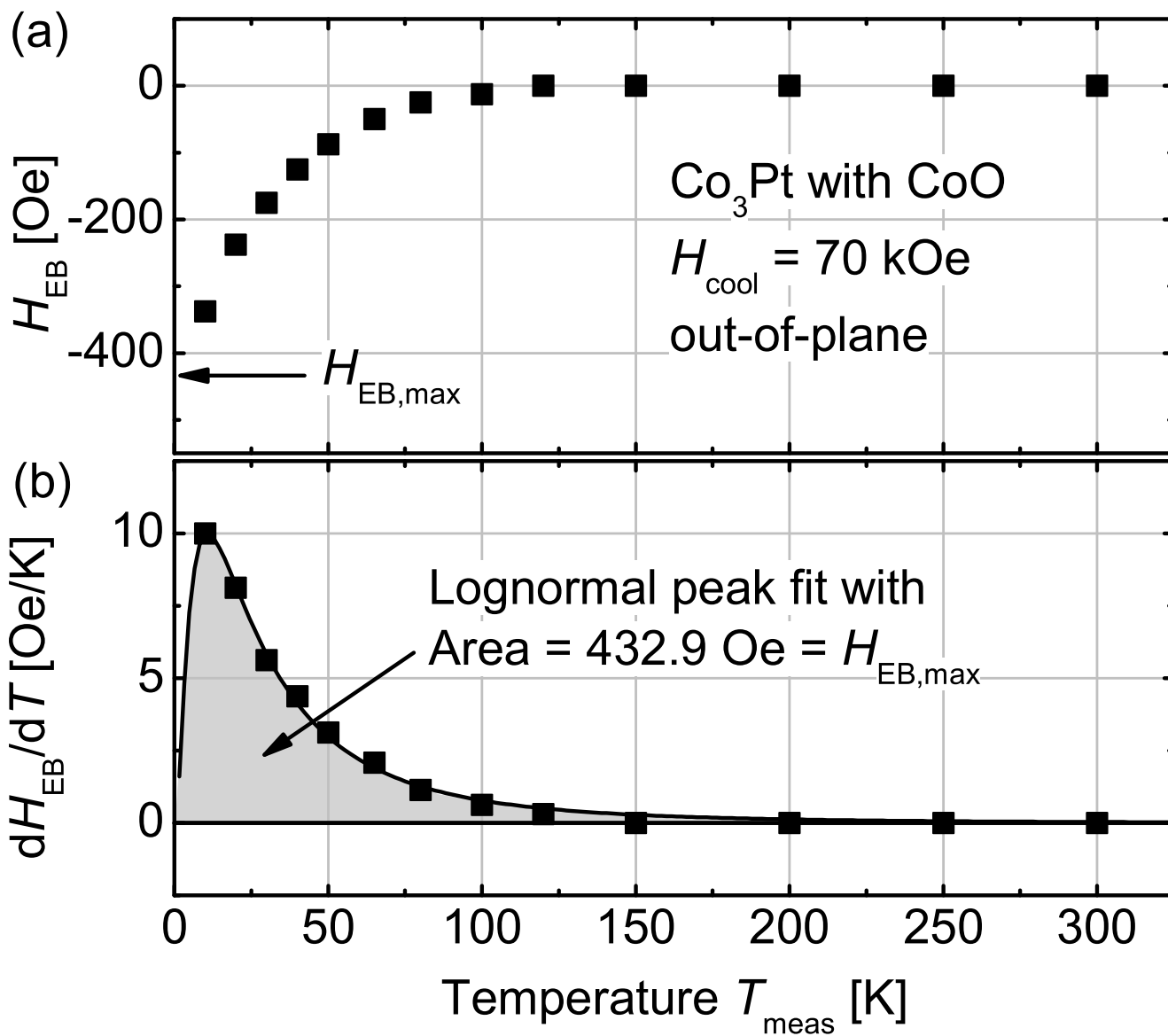


Figure 6ab (revision/figure6a\_6b.eps)

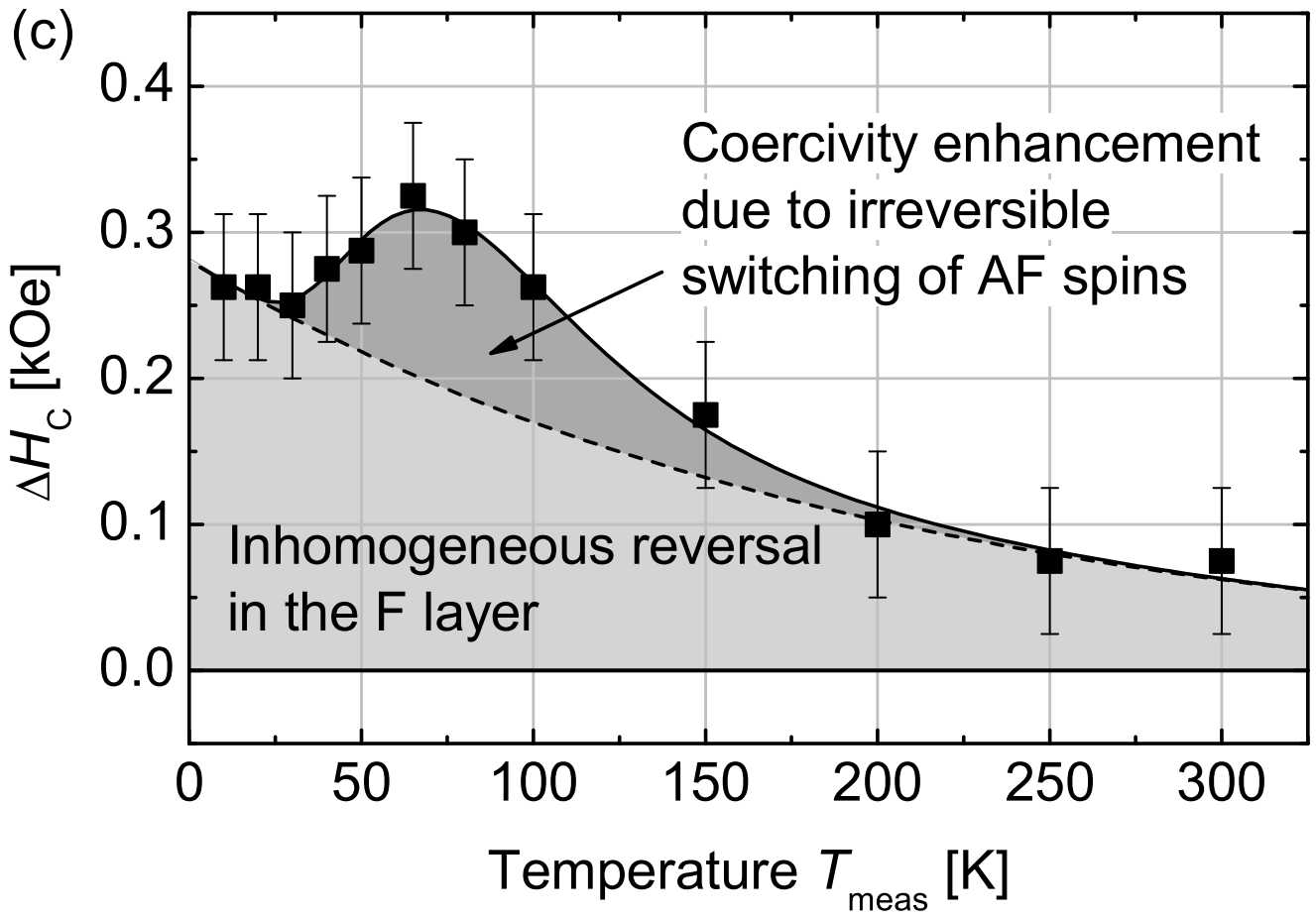


Figure 6c (revision/figure6c.eps)



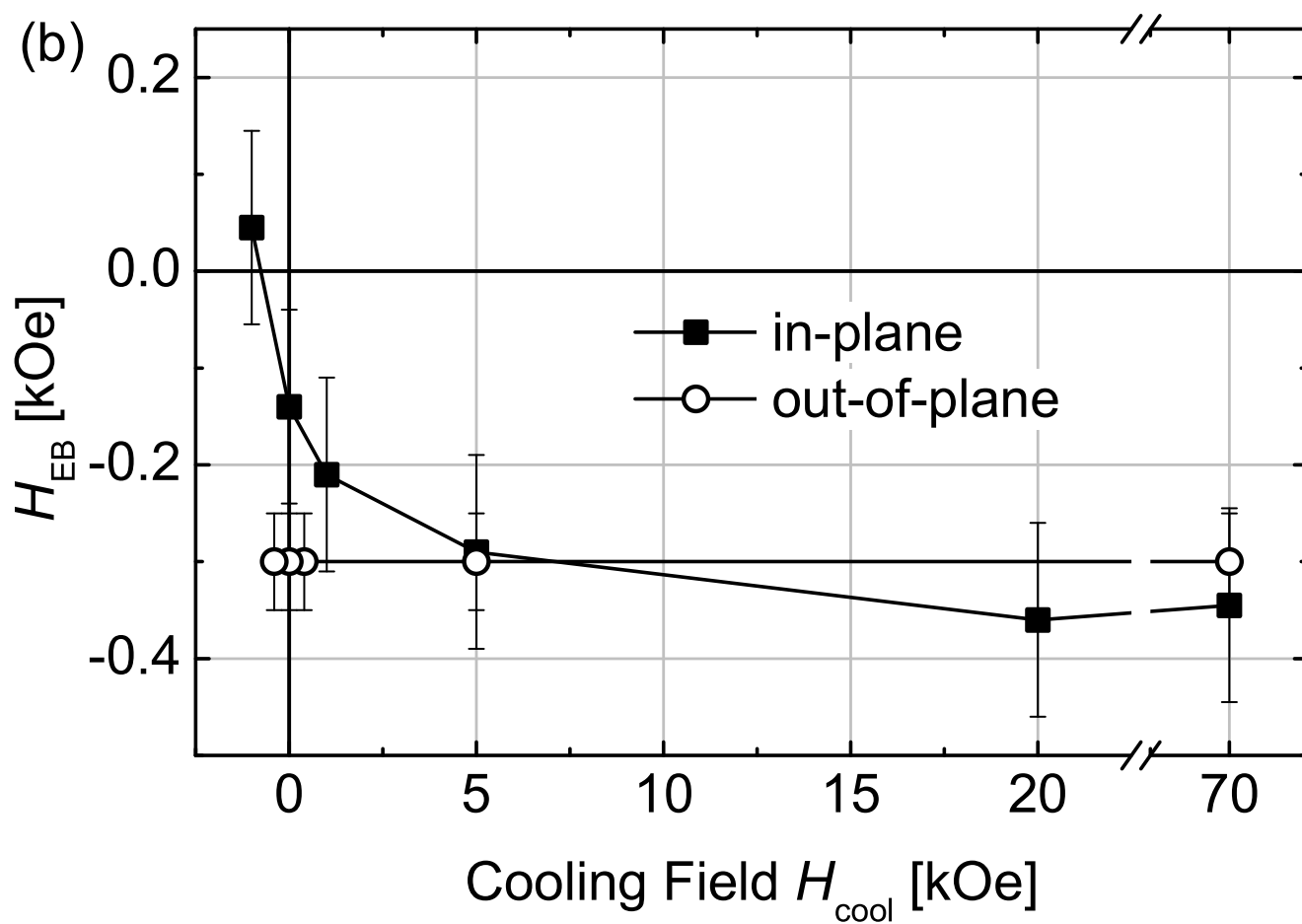


Figure 7b (revision/figure7b.eps)